Front. Earth Sci. 2016, 10(2): 264–273
DOI 10.1007/s11707-015-0517-4

RESEARCH ARTICLE

Interaction among controlling factors for landslides triggered by the 2008 Wenchuan, China Mw 7.9 earthquake

Lingling SHEN[1], Chong XU (✉)[2], Lianyou LIU[1]

1 Key Laboratory of Environment Change and Natural Disaster, MOE; State Key Laboratory of Earth Surface Processes and Resource Ecology, Academy of Disaster Reduction and Emergency Management, Beijing Normal University, Beijing 100875, China
2 Key Laboratory of Active Tectonics and Volcano, Institute of Geology, China Earthquake Administration, Beijing 100029, China

Abstract The 12 May 2008 Mw 7.9 Wenchuan, China earthquake triggered about 200,000 landslides, which were controlled by a number of factors. This study examines five factors: slope angle, slope aspect, lithology, peak ground acceleration (PGA), and fault side (relative position on the seismogenic fault, i.e., hanging wall or footwall), to determine how these factors control the co-seismic landslide occurrence and whether one or more factors, acting alone or in concert, are involved in promoting or suppressing landslides. We performed a multi-factor statistical analysis using data from the 2008 Wenchuan earthquake. The results show that in the areas characterized by steep topography or where strong ground shaking occurred during the earthquake, there is a closer relationship between slope aspect and landslide number density (LND) than other areas. The relationship between lithology and LND values depends on PGA. In turn, the relationship between LND values and PGA is also influenced by lithology. In addition, the controlling effect of lithology on co-seismic landslides on the hanging wall of the seismogenic fault is greater than that on the footwall. Examining interactions among these factors can improve understanding of the mechanisms of co-seismic landslide occurrence.

Keywords Wenchuan earthquake, co-seismic landslides, interaction among controlling factors, statistical analysis

1 Introduction

The May 12, 2008 Mw 7.9 Wenchuan, China earthquake occurred at the Longmen Shan Mountains, which forms the boundary between the eastern Tibetan Plateau to the west and the stable Sichuan basin to the east (Fig. 1). Based on interpretations of aerial photographs, remote sensing images, and field investigations, inventory compilation reveals that this event triggered more than 197,000 landslides around the NE-trending Longmen Shan fault, covering an area about 100,000 km^2 (Fig. 1) (Xu et al., 2013a, 2014a). As in earthquakes of similar magnitude, e.g., the October 17, 1989 California Loma Prieta Mw 6.9 earthquake in USA (Keefer, 2000), the January 17, 1994 Northridge Mw 6.7 in USA (Harp and Jibson, 1996), the 1999 Chi-chi Mw 7.6 in Taiwan, China (Liao et al., 2002; Wang et al., 2002), the October 23, 2004 Japan Niigata Mw 6.6 (Sato et al., 2005), the October 8, 2005 Kashmir Mw 7.6 (Sato et al., 2007), the 2010 Yushu of China Mw 6.9 (Xu et al., 2013b; Xu and Xu, 2014a), the 2010 Haiti Mw 7.0 (Gorum et al., 2013; Harp et al., 2013; Xu et al., 2014b), the 2013 Lushan of China Mw 6.6 (Xu, 2013; Xu and Xu, 2014b; Xu et al., 2015), the 2013 Minxian of China Mw 5.9 (Xu et al., 2013c, d, 2014c), as well as other events (Keefer, 1984; Harp et al., 2011; Guo and Hamada, 2013; Xu, 2014a, b), the occurrence of slope failures was controlled by a number of factors, which can be aggregated into three main categories: seismology, topography, and lithology. Each category contains several sub factors. Many studies of the Wenchuan earthquake (e.g., Dai et al., 2011; Gorum et al., 2011; Xu et al., 2014a) examine the relationships between these factors and co-seismic landslides, such as the slope angle and aspect (facing direction), distance to the fault, relative position on the fault (hanging wall or footwall), peak ground acceleration (PGA), and geological conditions (lithology, strata). However, most of the studies focused on correlations between individual factors and co-seismic landslides and did not examine the influence of these factors on the landslides. Do they work independently or interact with each other (promoting or suppressing each other)?

Received August 21, 2014; accepted January 26, 2015

E-mail: xuchong@ies.ac.cn,xc11111111@126.com

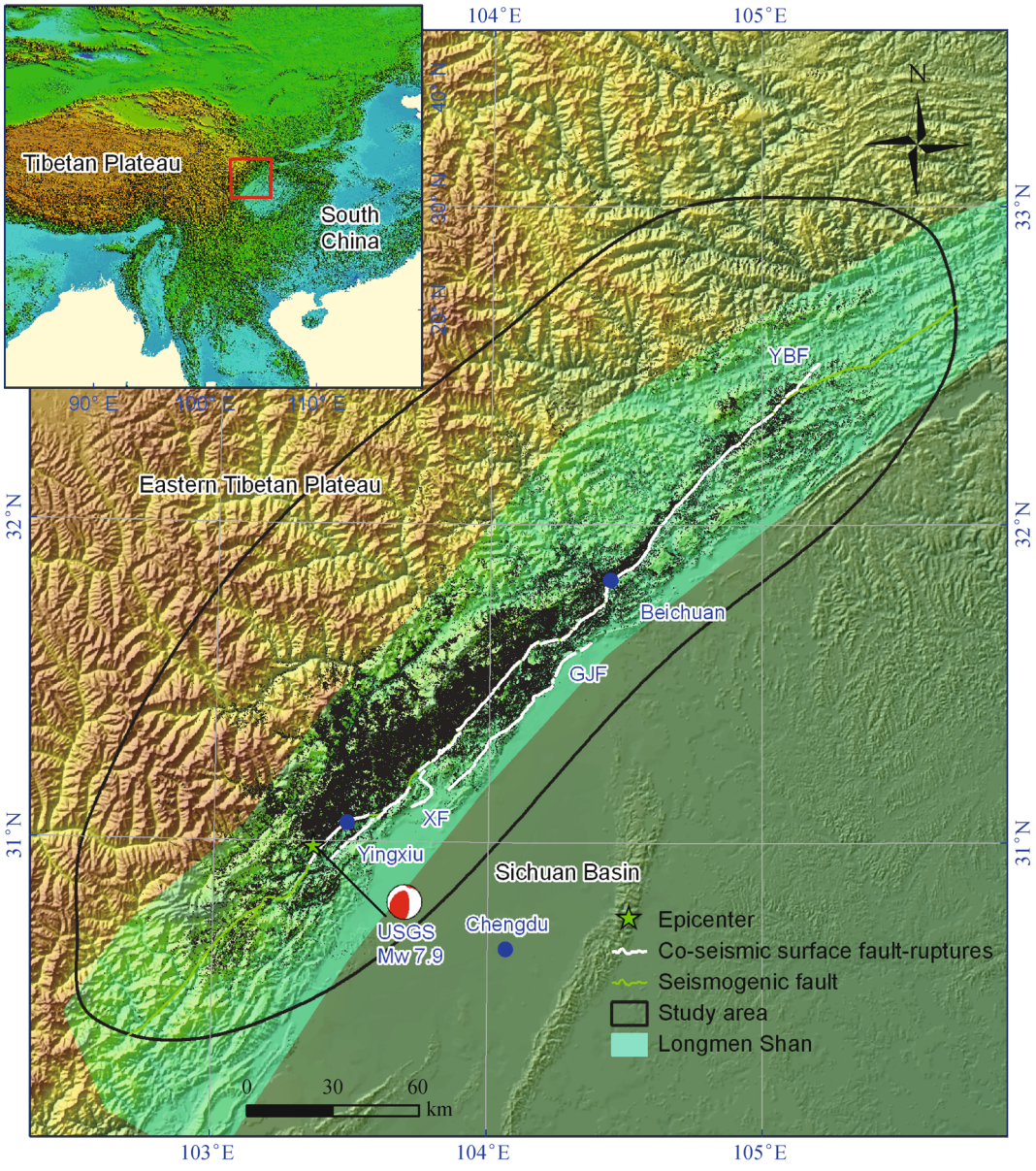

Fig. 1 Map showing landslides triggered by the 2008 Wenchuan Mw7.9 earthquake (black area) (modified from Xu et al. (2014a)). The black patches show the primary distribution of landslides. Box in inset is the study area of this work. White lines denote the major faults related with the Wenchuan major event. YBF, Yingxiu-Beichuan fault, GJF, Guanxian-Jiangyou fault, XF, Xiaoyudong fault (coseismic surface ruptures are from Xu et al. (2009a, b) and Tan et al. (2012)).

We used interactive statistical analysis to answer the above questions. We chose five controlling factors (slope angle, slope aspect, lithology, PGA, and relative position on the seismogenic fault) to examine how they influence the landslide number density of the area affected by the Wenchuan earthquake.

2 Data and method

Although the landslides triggered by the Wenchuan earthquake occurred in an area of about 100,000 km^2, the majority of them were concentrated in an oblong area along the NE-trending Longmen Shan fault, covering 44,031 km^2, and including 196,007 landslides (Xu et al., 2014a). We choose this as the study area (black oval in Fig. 1).

Topographic, geologic, and seismic factors have been widely used for landslide spatial analyses and hazard assessment (Kamp et al., 2008; Lee et al., 2008; Pradhan and Lee, 2010; Mansouri Daneshvar and Bagherzadeh, 2011; Bui et al., 2012; Kayastha, 2012; Pourghasemi et al., 2012a, b; Xu et al., 2012a, b). The study area terrain was mapped into eight slope aspect categories: north (N),

northeast (NE), east (E), southeast (SE), south (S), southwest (SW), west (W), and northwest (NW) (Fig. 2 (a)), with the aid of the "Surface Analysis" function of the "Spatial Analyst" tools on the ArcGIS platform. The correlation between slope aspect and landslide number density (LND) values shows that the eastern, southeastern, and southern directions are the orientations most conducive to co-seismic landslides during the 2008 Wenchuan event (Xu et al., 2014a). The slope angle in the study area includes four intervals: 0°–15°, 15°–30°, 30°–45°, and > 45° (Fig. 2(b)). The LND increases with slope angle. In other words, there is a positive correlation between LND and slope angle (Xu et al., 2014a). The LND values change greatly with different lithology features (Xu et al., 2014a). The lithology of the study area (Fig. 2(c)) is classified into four groups based on ascending LND values or susceptibilities (Table 1) (Xu et al., 2013a). The intensity of ground shaking during earthquakes can be measured by several indices, such as Arias intensity (Arias, 1970) and PGA. Although Arias intensity incorporates more information content in a single parameter and is more representative of the earthquake impact on slope stability than PGA (Harp and Wilson, 1995; Abdrakhmatov et al., 2003; Hwang et al., 2004) and has been widely used in recent years (Jibson, 1993; Miles and Ho, 1999; Jibson et al., 2000; Peláez et al., 2005; Hsieh and Lee, 2011; Chousianitis et al., 2014), PGA is still commonly used for correlating co-seismic landsides with the intensity of ground shaking in a number of recent studies (Liao and Lee, 2000; Carro et al., 2003; Khazai and Sitar, 2004; Lin et al., 2006; Xu and Xu, 2014a; Xu et al., 2014a, b). In most cases, Arias intensity is well correlated or has a

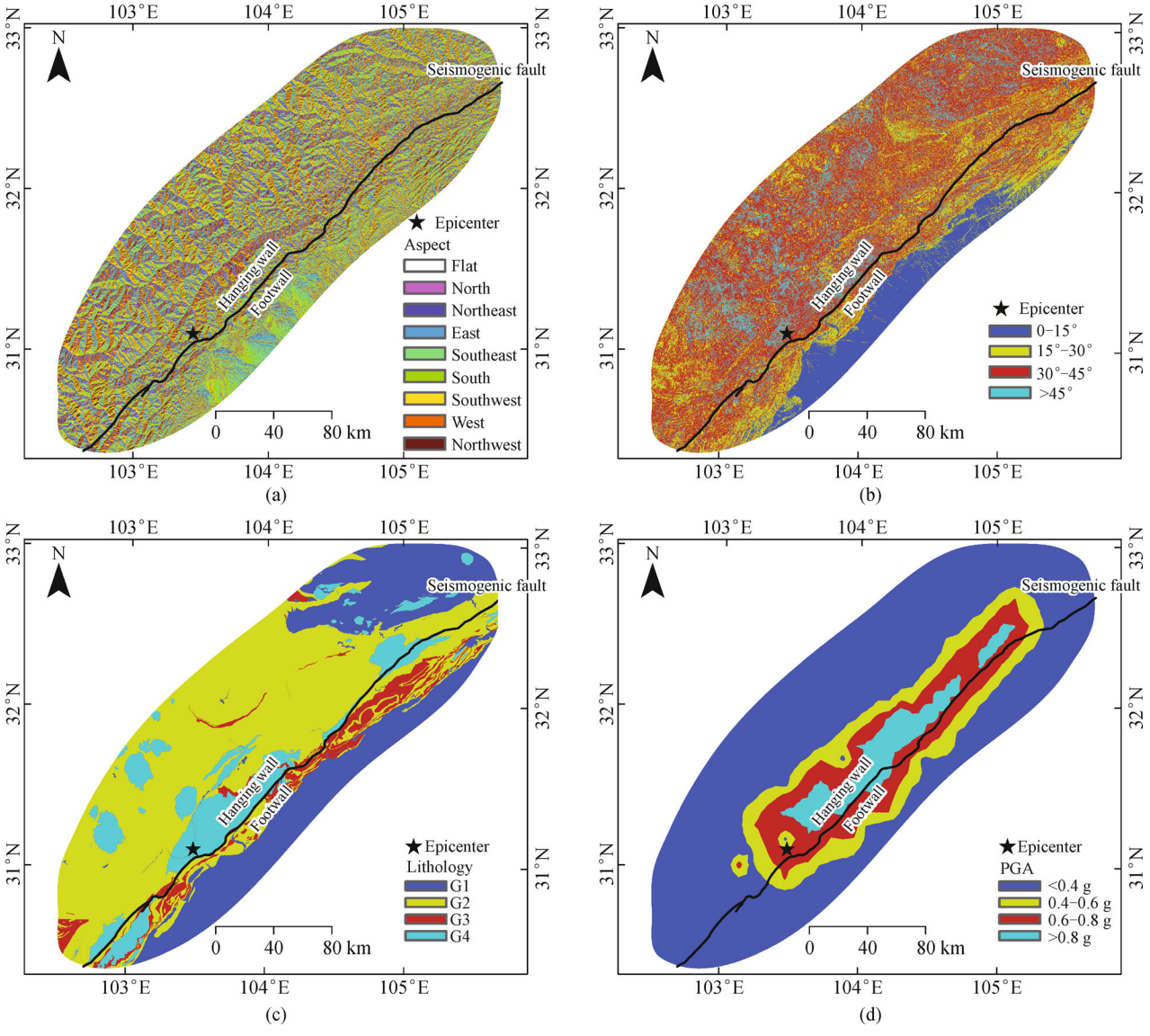

Fig. 2 Maps showing areal distributions of the four factors controlling co-seismic landslides triggered by the 2008 Wenchuan earthquake. (a) Slope aspect; (b) Slope angle; (c) Lithology; (d) PGA.

positive correlation with PGA (Romeo, 2000; Abdrakhmatov et al., 2003). Furthermore, although limited seismic station records related to the Wenchuan earthquake are available, only landslides triggered by the individual Wenchuan event are considered in this study. Therefore, we choose PGA for measuring the intensity of ground shaking in this study. The PGA data used here are from the website of US Geological Survey (2008), which are divided into four categories < 0.4 g, 0.4−0.6 g, 0.6−0.8g, and > 0.8 g (Fig. 2(d)). The LND values generally increase with increasing PGA values related to the Wenchuan earthquake (Xu et al., 2014a).

We assume that the LND value at any place of the study area is a function of one controlling factor, which may be influenced by another factor as well as by the relative position on the seismogenic fault (hanging wall or footwall). Based on the "Raster Calculator" module of the "Spatial Analyst" on the ArcGIS platform, DEM (digital elevation model) and the co-seismic landslide inventory map (Xu et al., 2014a), we take the LND value of one factor category as the dominant variable while using another category and hanging wall/footwall as secondary variables. This results in a group of curves which display how the LND changes with the dominant variable and whether such a change is influenced by the secondary variables. For example, the LND values of each slope aspect category are determined corresponding to four slope angle categories and the hanging wall/footwall respectively (Figs. 3(a) and 3(b)). In the two panels, we can observe how LND varies with the slope aspect and whether it is influenced by slope angle category and hanging wall/footwall. A statistical analysis for each factor category is made (Figs. 3−6), which allows us to examine whether or how these factors interact with each other. Actually, such a statistical process is equivalent to a multiple-factor interactive analysis which may reveal the mutual effect among the controlling factors.

3 Results

3.1 Influence of slope angles and fault sides

First, we examined whether slope angles and fault sides have an impact on the correlations between LND and the other three factors, including slope aspect, lithology, and PGA (Fig. 3). We found that when the slope angles are smaller, LND values change little with slope aspect, which holds true for both the hanging wall and footwall of the fault (Figs. 3(a) and 3(b)). When the slope angle becomes larger, LND values of slope aspects toward south (S) and southeast (SE) are more conspicuous on both the hanging wall and footwall of the seismogenic fault. In other words, the slope aspect effect is more notable in areas with higher slope angles (Figs. 3(a) and 3(b)). LND increases as lithology changes from G1 to G4 for each slope-angle category (Fig. 3(c)), and such a change is more significant with increasing slope angles on the hanging wall of the fault. We noted an abnormal variation which appears on the footwall, where the LND values for G3 exceed those for G4 (Fig. 3(d)), which differs from the pattern on the hanging wall. LND values also rise with increasing PGA; the greater the slope angle, the faster the LND rises with PGA on both the hanging wall and footwall of the fault (Figs. 3(e) and 3(f)). We found that when PGA is over 0.8 g, the LND for slope angles greater than 45° on the footwall is greater than that on the hanging wall (Figs. 3(e) and 3(f)).

3.2 Influence of slope aspects and fault sides

Overall, the LND values rise consistently with increasing slope angles, lithology categories G1 to G4, and PGA for both fault sides (Fig. 4), which shows that slope aspect has little influence. The only exception is that the LND values in lithology type G4 are less than those in G3 on the footwall (Fig. 4(d)), which is inconsistent with the LND-based definition of lithology groups (Table 1). Figures 4(c) and 4(d) indicate that LND values for G4 on the hanging wall are larger than those of the footwall, which shows stronger controls by lithology on the co-seismic landslides of the hanging wall than those of the footwall, regardless of slope aspect. On the contrary, LND values in areas with strong ground shaking of the footwall are larger than those of the hanging wall. Such a phenomenon shows that there is a stronger control by PGA on the landslides of the footwall than that of the hanging wall.

Table 1 Lithology combinations of the study area (Xu et al., 2013a)

No.	Geological periods	Lithology	LND interval /(km^{-2})	Average LND /(km^{-2})	Landslide susceptibility
G1	Q, N−K, J, C2, PZ1	Quaternary deposits, conglomerates, sandstone, limestone, and quartz sandstone	0.09−0.77	0.42	Low
G2	T2, C−P, D2, S1, S2, O	Limestone, phyllite, sandstone, and marl	1.9−4.1	2.78	Moderate
G3	P1, P2, C1, D1	Dense structure of limestone, dolomitic limestone, and shale	7.1−8.8	8.59	High
G4	T1, Є, Z, PZ2, PZ3	Sandstone, schist and andesite, granitic rocks, and thick layer of limestone	12.2−19.1	17.2	Very high

Note: Q, Quaternary; N−K, Neogene, Paleogene, and Cretaceous; J, Jurassic; T, Triassic; P, Permian; C, Carboniferous; D, Devonian; S, Silurian; O, Ordovician; Є, Cambrian; Z, Sinian; PZ, Presinian. LND, landslide number density.

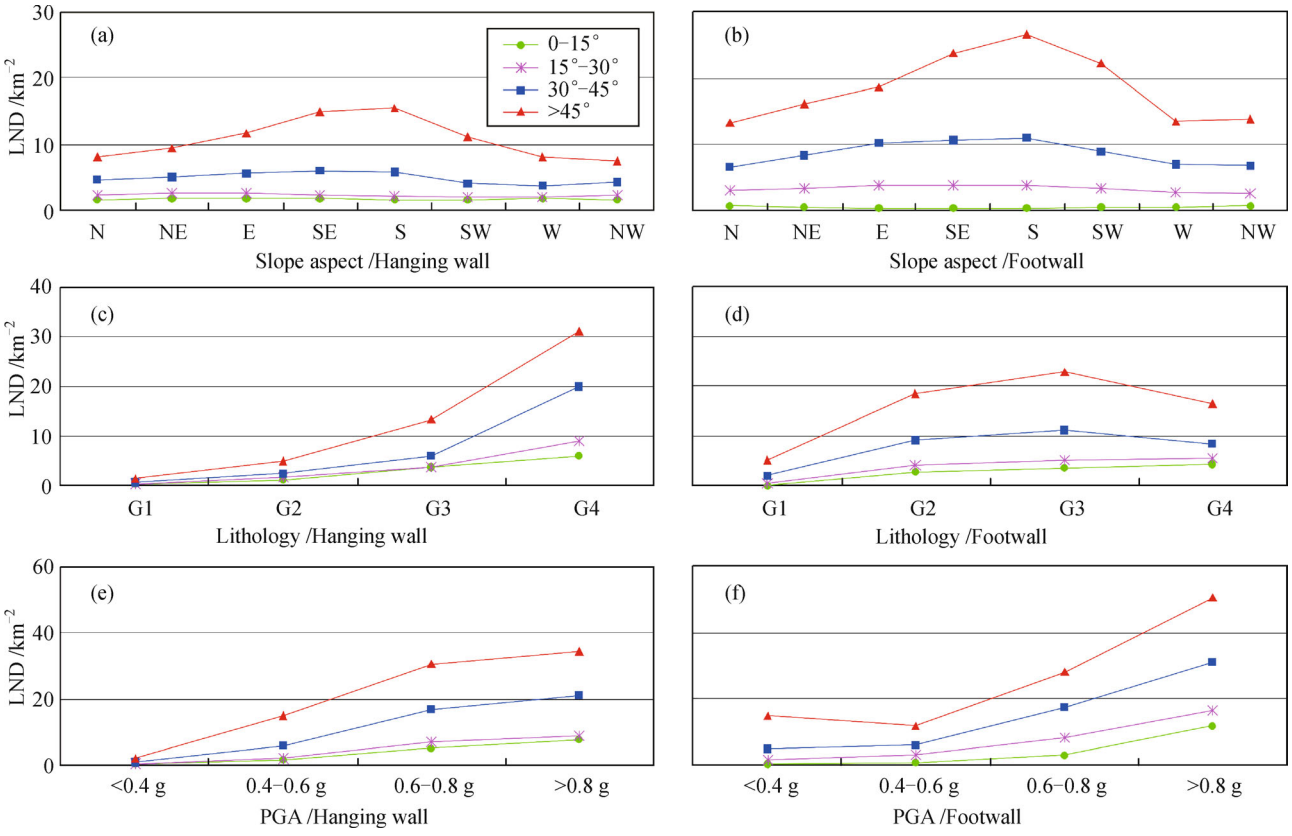

Fig. 3 Average landslide number density (LND) versus slope aspect, lithology, and peak ground acceleration (PGA) for different slope angle categories (inset in (a)). Definitions of lithologies are listed in Table 1. Note: (a), (c), and (e) correspond to the areas in the hanging wall side, and (b), (d), and (f) for areas in the footwall side.

3.3 Influence of lithology and fault sides

LND has a positive correlation with slope angle in every lithology combination (G1 to G4), especially for the areas in the hanging wall side (Figs. 5(a) and 5(b)). At first glance, Fig. 5(a), for G3 and G4, the LND values of slopes with higher angles are much larger than those of slopes with lower angles, whereas the influence of slope angle on LND for G1 and G2 is very small. Indeed, the ratio of LND values of slope angles $> 45°$ and $< 15°$ on the hanging wall for G1 to G4 are similar and equal to 1.28/0.28 (4.6), 4.78/1.13 (4.25), 13.21/3.52 (3.76), and 31.1/5.74 (5.42). This means that differences in lithology do not influence the controlling role of slope steepness in generation of landslides. LND changes little with varied slope aspects for lithology, and differences in LND among lithologies G1 to G4 seem larger on the hanging wall than that on the footwall (Figs. 5(c) and 5(d)). As shown in Figs. 5(e) and 5(f), in the four lithology categories, LND varies with PGA in a relatively complex manner, particularly on the hanging wall (Figs. 5(e) and 5(f)). This may indicate the possible influence of geologic conditions on the relationship between PGA and landslides. But this appears to occur only on the hanging wall, rather than on the footwall.

3.4 Influence of PGA and fault sides

From Figs. 6(a) and 6(b), it can be observed that PGA has little influence on the relationship between LND and slope angle. From panels 6(c) and 6(d), there are obvious differences in correlations between LND values and slope aspect in different PGA classes. In the hanging wall areas with PGA > 0.6 g, an obvious aspect effect is present, implying that co-seismic landslides are more likely to occur in areas with east, southeast, and south slope aspects. A similar pattern is also seen in the footwall area (Fig. 6(d)). It shows that the aspect effect is mainly present in those areas of PGA > 0.8 g. Although there is no clear correlation of landslide densities with slope aspects in the hanging wall and footwall sides, the graphs still indicate that as PGA values increase, the slope aspect effect on co-seismic landslides becomes more obvious. In addition, in the areas with stronger ground motion (PGA > 0.8 g), LND on the footwall is greater than that on the hanging wall. As in Fig. 5(e), the relationship between LND and lithology also exhibits complicated variations on the hanging wall (Fig. 6(e)), though not as notable on the footwall (Fig. 6(f)). This indicates the obvious effects of lithology on correlations between co-seismic landslides

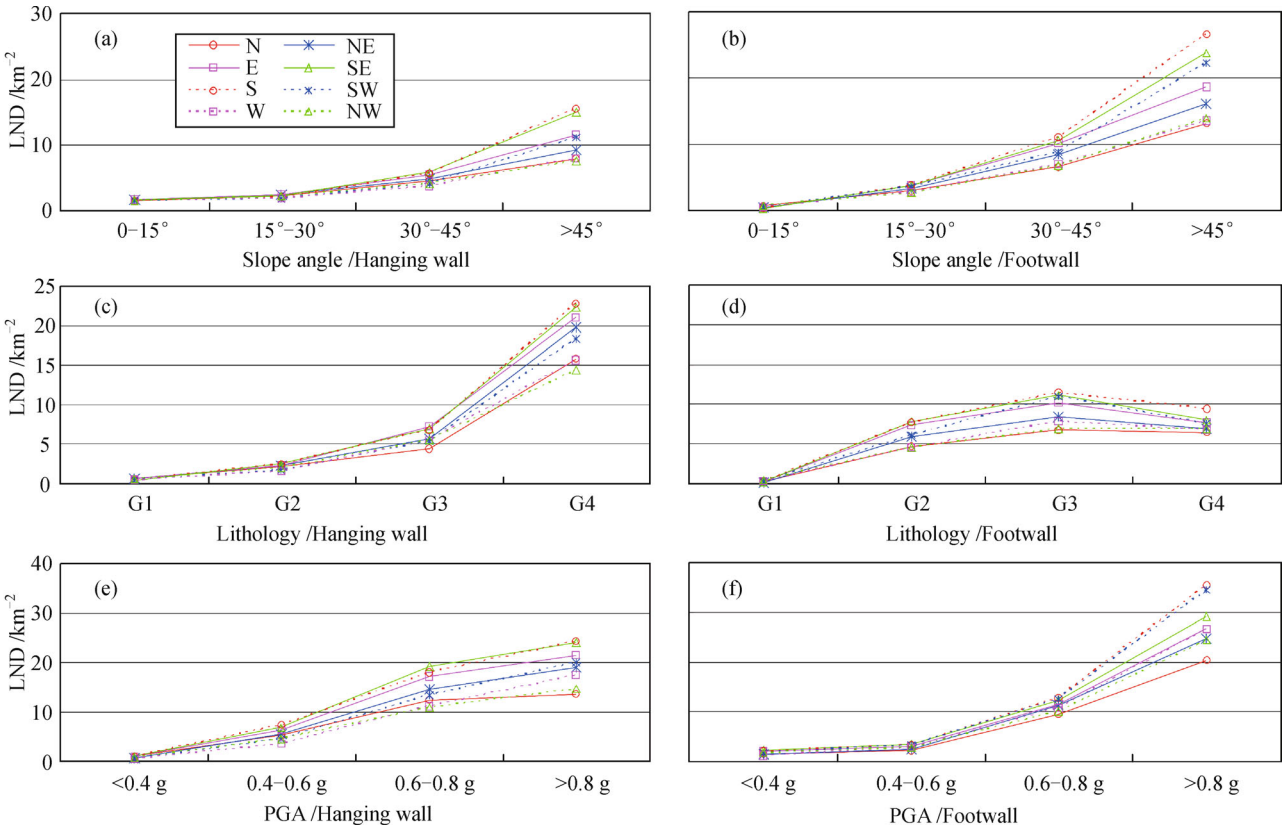

Fig. 4 Average landslide number density (LND) versus slope angle category, lithology, and peak ground acceleration (PGA) for different slope aspects (inset in (a)). Definitions of lithology groups are listed in Table 1. Note: (a), (c), and (e) correspond to areas that lie in the hanging wall side, and (b), (d), and (f) for areas in the footwall side.

and PGA values in the hanging wall side. Similarly, it also reveals that the degree of ground shaking can also have an influence on the relationship between lithology and co-seismic landslide densities.

4 Discussion

The slope aspect effect shows that landslides are more likely on certain slope aspects, whether or not the landslides are triggered by earthquakes or other factors. However, the mechanisms of such effects are inconclusive. Previous studies on non-seismic landslides suggest that the slope aspect effect is perhaps due to the differences of exposure to sunlight, drying winds, rainfall (degree of saturation), discontinuities, insolation (weathering), weather conditions (precipitation, snow melt water), land cover (forest, grassland, brush land, agricultural land), and soil conditions (infiltration capacity) in different slopes aspects (Kamp et al., 2008; Yalcin, 2008; Bui et al., 2012). Recent studies demonstrate that the slope aspect effect of co-seismic landslides could be related to the movement direction of the hanging wall, which presumably results from the direction of seismic wave propagation or the inertia of geological blocks. This seems to have occurred in a few earthquakes, such as the 2008 Wenchuan (Xu et al., 2014a), the 2013 Lushan (Xu and Xiao, 2013), the 2010 Yushu (Xu and Xu, 2014a), and the 2010 Haiti (Xu et al., 2014b) events. However, it is still difficult to determine which mechanism is responsible for the slope aspect effect.

This study shows that the slope aspect effect in areas with steeper topography is more significant than in areas with smaller slope angles. Similarly, the slope aspect effect is also more obvious in areas with larger PGA values than in those with smaller PGA values. This phenomenon would not exist if the slope aspect effect were generated solely by topographic, geologic, or weather conditions (Kamp et al., 2008; Yalcin, 2008) since the slope aspect effect changes with topography. Furthermore, the seismic wave amplification can be caused by topographic differences (Meunier et al., 2008). Therefore, the slope aspect effect in the 2008 Wenchuan earthquake is most likely due to seismic factors, including seismic wave propagation, the inertia of geological blocks, and crustal stress.

Lithology can influence the relationship between PGA and LND. The effect of PGA on co-seismic landslides shows obvious differences among lithology categories (Figs. 5(e) and 5(f)). On the other hand, PGA can also influence the relationship between lithology and LND. For example, for certain PGA, the relationship between LND

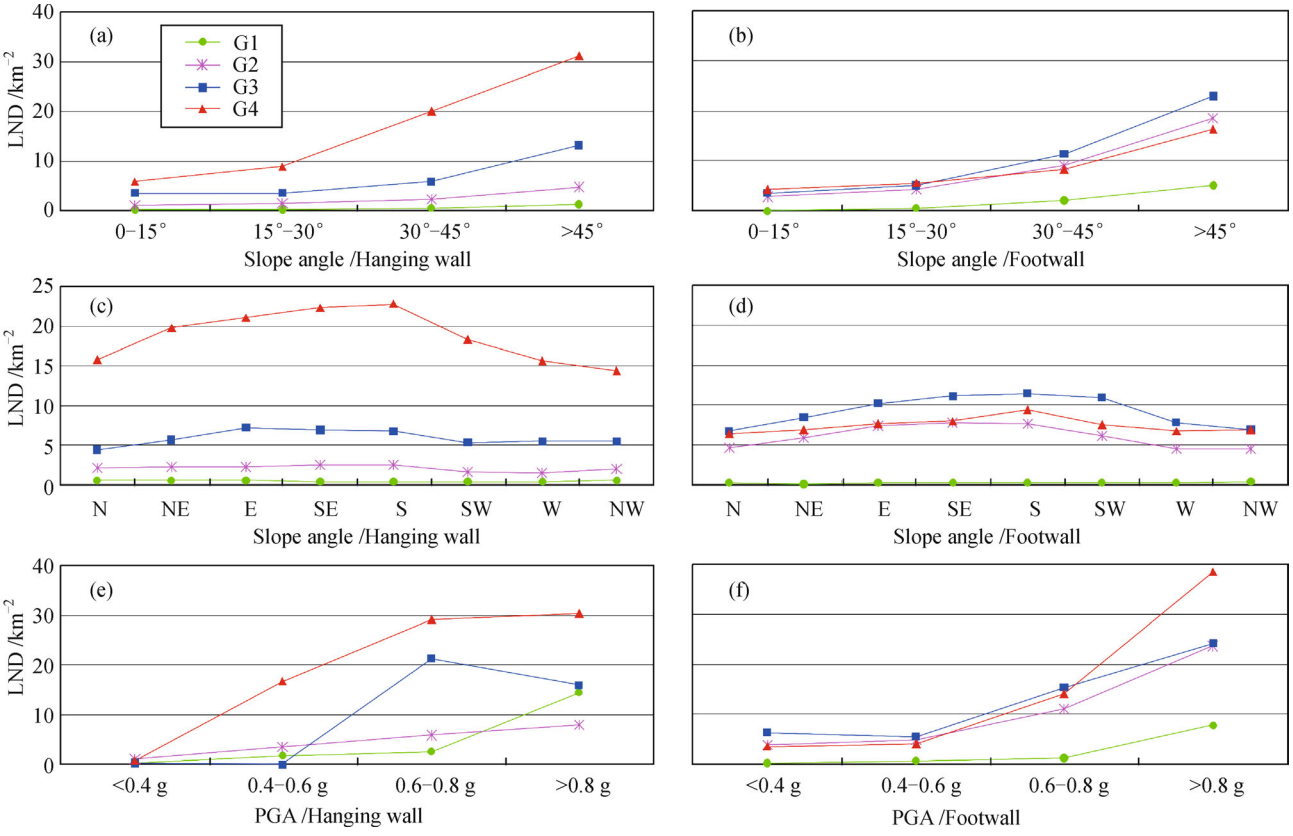

Fig. 5 Average landslide number density (LND) versus slope angle category, slope aspect, and peak ground acceleration (PGA) for different lithology groups (inset in (a)). Definitions of lithologies are listed in Table 1. Note: (a), (c), and (e) correspond to areas that lie in the hanging wall side, and (b), (d), and (f) for areas in the footwall side.

and lithology generally shows similar tendencies. However, sudden changes may occur if the PGA reaches certain thresholds (Figs. 6(e) and 6(f)). This indicates the complex mechanisms of PGA and lithology controlling co-seismic landslides.

Based on the "Band Collection Statistics" module of the "Spatial Analyst Tools" in the ArcToolbox, we conducted a simple spatial correlation analysis to the five factors (slope angle, slope aspect, lithology, PGA and two fault sides) (Table 2). The value of 1 indicates a perfect positive correlation between two factors, −1 stands for a perfect negative correlation, and 0 means no correlation. The closer the value is to zero, the lower the degree of spatial correlation between the two factors. It can be observed that all the spatial correlations of the five thematic layers are low. However, our analysis in the last section reveals a series of interactive influences among the factors that affect earthquake-induced landslides. Therefore, the limitations of the simple spatial correlation analysis should be examined in future studies.

5 Conclusions

We performed interactive analysis of five factors on 196,007 landslides triggered by the 2008 Wenchuan earthquake. The results show that the slope aspect effect on co-seismic landslides is more obvious in the areas with steeper topography or stronger ground shaking. In addition, the relationships between slope aspects and LND show similar tendencies for different lithology categories. This indicates that the slope aspect effect of co-seismic landslides (Xu and Xiao, 2013; Xu and Xu, 2014a; Xu et al., 2014a, b) is different from those of non-seismic landslides (Kamp et al., 2008; Yalcin, 2008). The slope aspect effects of non-seismic landslides are caused mainly by differences in vegetation cover, light, rainfall, and soil conditions in different slope aspects, while those of co-seismic landslides are primarily associated with seismic factors such as the directions of geological block movement, crustal stress, and seismic wave propagation.

The results of this study show that lithology can influence the relationship between PGA and LND. Conversely, PGA can also have an influence on the performance of lithology affecting co-seismic landslides. LND values under several factors have significant differences from the hanging wall to footwall. For instance, on the footwall with steeper topography (slope angle > 30°), LND values are higher than those on the hanging wall with steeper topography. LNDs of high landslide-

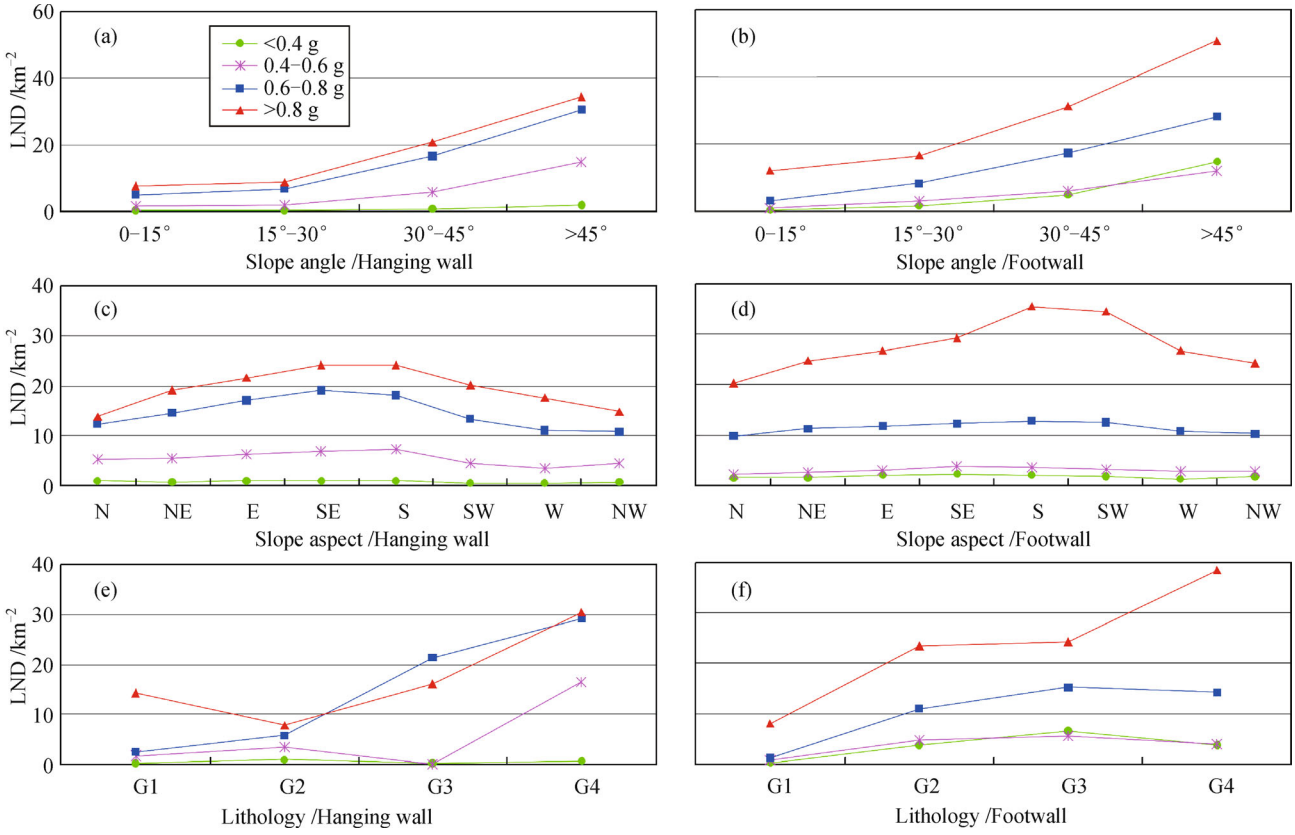

Fig. 6 Average landslide number density (LND) versus slope angle category, slope aspect and lithology for PGA categories (inset in (a)). Definitions of lithology are listed in Table 1. Note: (a), (c), and (e) correspond to areas that lie in the hanging wall side, and (b), (d), and (f) for areas in the footwall side.

Table 2 A simple analysis of spatial correlation for the five factors related to coseismic landslides

Layer	Slope angle	Slope aspect	Lithology	PGA	Fault side
Slope angle	1	0.01636	0.2851	0.08105	−0.45053
Slope aspect		1	0.01315	0.00088	−0.01135
Lithology			1	0.38258	−0.1739
PGA				1	−0.04488
Fault side					1

prone lithology categories are more prominent on the hanging wall than those on the footwall, which indicates that the controlling effect of lithology on co-seismic landslides on the hanging wall is more intense than that on the footwall. Although the spatial correlation analysis of the five factors shows weak correlations between them, our analyses show that there are interactive correlations among these controlling factors.

Acknowledgements This research was supported by the National Natural Science Foundation of China (Grant Nos. 41472202 and 41202235) and the National Basic Research Program of China (No. 2012BAK10B03). Comments from three anonymous reviewers significantly improved this manuscript.

References

Abdrakhmatov K, Havenith H B, Delvaux D, Jongmans D, Trefois P (2003). Probabilistic PGA and arias intensity maps of Kyrgyzstan (Central Asia). J Seismol, 7(2): 203–220

Arias A (1970) A measure of earthquake intensity. In: Hansen R J, ed. Seismic Design for Nuclear Power Plants. Cambridge: Massachusetts Inst. of Tech., 438–483

Bui D T, Pradhan B, Lofman O, Revhaug I, Dick O B (2012). Spatial prediction of landslide hazards in Hoa Binh province (Vietnam): a comparative assessment of the efficacy of evidential belief functions and fuzzy logic models. Catena, 96: 28–40

Carro M, De Amicis M, Luzi L, Marzorati S (2003). The application of

predictive modeling techniques to landslides induced by earthquakes: the case study of the 26 September 1997 Umbria–Marche earthquake (Italy). Eng Geol, 69(1–2): 139–159

Chousianitis K, Del Gaudio V, Kalogeras I, Ganas A (2014). Predictive model of Arias intensity and Newmark displacement for regional scale evaluation of earthquake-induced landslide hazard in Greece. Soil Dyn Earthquake Eng, 65: 11–29

Dai F C, Xu C, Yao X, Xu L, Tu X B, Gong Q M (2011). Spatial distribution of landslides triggered by the 2008 Ms 8.0 Wenchuan earthquake, China. J Asian Earth Sci, 40(4): 883–895

Mansouri Daneshvar M R, Bagherzadeh A (2011). Landslide hazard zonation assessment using GIS analysis at Golmakan Watershed, northeast of Iran. Front Earth Sci, 5(1): 70–81

Gorum T, Fan X M, van Westen C J, Huang R Q, Xu Q, Tang C, Wang G H (2011). Distribution pattern of earthquake-induced landslides triggered by the 12 May 2008 Wenchuan earthquake. Geomorphology, 133(3–4): 152–167

Gorum T, van Westen C J, Korup O, van der Meijde M, Fan X M, van der Meer F D (2013). Complex rupture mechanism and topography control symmetry of mass-wasting pattern, 2010 Haiti earthquake. Geomorphology, 184: 127–138

Guo D P, Hamada M (2013). Qualitative and quantitative analysis on landslide influential factors during Wenchuan earthquake: a case study in Wenchuan County. Eng Geol, 152(1): 202–209

Harp E L, Jibson R W (1996). Landslides triggered by the 1994 Northridge, California, earthquake. Bull Seismol Soc Am, 86(1B): S319–S332

Harp E L, Jibson R W, Dart R L (2013). The effect of complex fault rupture on the distribution of landslides triggered by the 12 January 2010, Haiti earthquake. Landslide Science and Practice: 157–161

Harp E L, Keefer D K, Sato H P, Yagi H (2011). Landslide inventories: the essential part of seismic landslide hazard analyses. Eng Geol, 122 (1–2): 9–21

Harp E L, Wilson R C (1995). Shaking intensity thresholds for rock falls and slides: evidence from 1987 Whittier Narrows and Superstition Hills Earthquake strong-motion records. Bull Seismol Soc Am, 85 (6): 1739–1757

Hsieh S Y, Lee C T (2011). Empirical estimation of the Newmark displacement from the Arias intensity and critical acceleration. Eng Geol, 122(1–2): 34–42

Hwang H, Lin C K, Yeh Y T (2004) Derivation of attenuation relations of Arias Intensity using the Chi-chi earthquake data. In: Proceedings of the 13th World Conference on Earthquake Engineering, Paper No. 3108

Jibson R W (1993). Predicting earthquake-induced landslide displacements using Newmark's sliding block analysis. Transp Res Rec, 1411: 9–17

Jibson R W, Harp E L, Michael J A (2000). A method for producing digital probabilistic seismic landslide hazard maps. Eng Geol, 58(3–4): 271–289

Kamp U, Growley B J, Khattak G A, Owen L A (2008). GIS-based landslide susceptibility mapping for the 2005 Kashmir earthquake region. Geomorphology, 101(4): 631–642

Kayastha P (2012). Application of fuzzy logic approach for landslide susceptibility mapping in Garuwa sub-basin, East Nepal. Front Earth Sci, 6(4): 420–432

Keefer D K (1984). Landslides caused by earthquakes. Geol Soc Am Bull, 95(4): 406–421

Keefer D K (2000). Statistical analysis of an earthquake-induced landslide distribution —the 1989 Loma Prieta, California event. Eng Geol, 58(3–4): 231–249

Khazai B, Sitar N (2004). Evaluation of factors controlling earthquake-induced landslides caused by Chi-Chi earthquake and comparison with the Northridge and Loma Prieta events. Eng Geol, 71(1–2): 79–95

Lee C T, Huang C C, Lee J F, Pan K L, Lin M L, Dong J J (2008). Statistical approach to earthquake-induced landslide susceptibility. Eng Geol, 100(1–2): 43–58

Liao C, Liao H, Lee C (2002). Statistical analysis of factors affecting landslides triggered by the 1999 Chi-Chi earthquake, Taiwan. American Geophysical Union, Fall Meeting 2002, abstract #H12D-0951, http://adsabs.harvard.edu/abs/2002AGUFM.H12D0951L

Liao H W, Lee C T (2000) Landslides triggered by the Chi-Chi earthquake. In: Proceedings of the 21st Asian Conference on Remote Sensing, Taipei, 1–2: 383–388

Lin C W, Liu S H, Lee S Y, Liu C C (2006). Impacts of the Chi-Chi earthquake on subsequent rainfall-induced landslides in central Taiwan. Eng Geol, 86(2–3): 87–101

Meunier P, Hovius N, Haines A J (2008). Topographic site effects and the location of earthquake induced landslides. Earth Planet Sci Lett, 275(3–4): 221–232

Miles S B, Ho C L (1999). Rigorous landslide hazard zonation using Newmark's method and stochastic ground motion simulation. Soil Dyn Earthquake Eng, 18(4): 305–323

Peláez J A, Delgado J, López Casado C (2005). A preliminary probabilistic seismic hazard assessment in terms of Arias intensity in southeastern Spain. Eng Geol, 77(1–2): 139–151

Pourghasemi H R, Mohammady M, Pradhan B (2012a). Landslide susceptibility mapping using index of entropy and conditional probability models in GIS: Safarood Basin, Iran. Catena, 97: 71–84

Pourghasemi H R, Pradhan B, Gokceoglu C (2012b). Application of fuzzy logic and analytical hierarchy process (AHP) to landslide susceptibility mapping at Haraz watershed, Iran. Nat Hazards, 63(2): 965–996

Pradhan B, Lee S (2010). Regional landslide susceptibility analysis using back-propagation neural network model at Cameron Highland, Malaysia. Landslides, 7(1): 13–30

Romeo R (2000). Seismically induced landslide displacements: a predictive model. Eng Geol, 58(3–4): 337–351

Sato H P, Hasegawa H, Fujiwara S, Tobita M, Koarai M, Une H, Iwahashi J (2007). Interpretation of landslide distribution triggered by the 2005 Northern Pakistan earthquake using SPOT 5 imagery. Landslides, 4(2): 113–122

Sato H P, Sekiguchi T, Kojiroi R, Suzuki Y, Iida M (2005). Overlaying landslides distribution on the earthquake source, geological and topographical data: the Mid Niigata prefecture earthquake in 2004, Japan. Landslides, 2(2): 143–152

Tan X B, Yuan R M, Xu X W, Chen G H, Klinger Y, Chang C P, Ren J J, Xu C, Li K (2012). Complex surface rupturing and related formation mechanisms in the Xiaoyudong area for the 2008 Mw 7.9 Wenchuan Earthquake, China. J Asian Earth Sci, 58: 132–142

US Geological Survey (2008). Shakemap us2008ryan. http://earthquake.

usgs.gov/earthquakes/shakemap/global/shake/2008ryan/.

Wang W N, Nakamura H, Tsuchiya S, Chen C C (2002). Distributions of landslides triggered by the Chi-chi Earthquake in Central Taiwan on September 21, 1999. Landslides- Journal of the Japan Landslide Society, 38(4): 318–326

Xu C (2013). Assessment of earthquake-triggered landslide susceptibility based on expert knowledge and information value methods: a case study of the 20 April 2013 Lushan, China Mw6.6 earthquake. Disaster Advances, 6(13): 119–130

Xu C (2014a). Do buried-rupture earthquakes trigger less landslides than surface-rupture earthquakes for reverse faults? Geomorphology, 216: 53–57

Xu C (2014b). Preparation of earthquake-triggered landslide inventory maps using remote sensing and GIS technologies: principles and case studies. Geoscience Frontiers, doi: 10.1016/j.gsf.2014.03.004

Xu C, Dai F C, Xu X W, Lee Y H (2012a). GIS-based support vector machine modeling of earthquake-triggered landslide susceptibility in the Jianjiang River watershed, China. Geomorphology, 145–146: 70–80

Xu C, Shyu J B H, Xu X W (2014b). Landslides triggered by the 12 January 2010 Port-au-Prince, Haiti, Mw = 7.0 earthquake: visual interpretation, inventory compiling, and spatial distribution statistical analysis. Nat Hazards Earth Syst Sci, 14(7): 1789–1818

Xu C, Xiao J Z (2013). Spatial analysis of landslides triggered by the 2013 Ms 7.0 Lushan earthquake: a case study of a typical rectangle area in the northeast of Taiping town. Seismology and Geology, 35 (2): 436–451 (in Chinese)

Xu C, Xu X, Shyu J B H, Gao M, Tan X, Ran Y, Zheng W (2015). Landslides triggered by the 20 April 2013 Lushan, China, Mw 6.6 earthquake from field investigations and preliminary analyses. Landslides, 12(2): 365–385

Xu C, Xu X W (2014a). Statistical analysis of landslides caused by the Mw 6.9 Yushu, China, earthquake of April 14, 2010. Nat Hazards, 72 (2): 871–893

Xu C, Xu X W (2014b). The spatial distribution pattern of landslides triggered by the 20 April 2013 Lushan earthquake of China and its implication to identification of the seismogenic fault. Chin Sci Bull, 59(13): 1416–1424

Xu C, Xu X W, Dai F C, Saraf A K (2012b). Comparison of different models for susceptibility mapping of earthquake triggered landslides related with the 2008 Wenchuan earthquake in China. Comput Geosci, 46: 317–329

Xu C, Xu X W, Shyu J B H, Zheng W J, Min W (2014c). Landslides triggered by the 22 July 2013 Minxian-Zhangxian, China, Mw 5.9 earthquake: inventory compiling and spatial distribution analysis. J Asian Earth Sci, 92: 125–142

Xu C, Xu X W, Yao Q, Wang Y Y (2013a). GIS-based bivariate statistical modelling for earthquake-triggered landslides susceptibility mapping related to the 2008 Wenchuan earthquake, China. Quarterly Journal of Engineering Geology and Hydrogeology, 46(2): 221–236

Xu C, Xu X W, Yao X, Dai F C (2014a). Three (nearly) complete inventories of landslides triggered by the May 12, 2008 Wenchuan Mw 7.9 earthquake of China and their spatial distribution statistical analysis. Landslides, 11(3): 441–461

Xu C, Xu X W, Yu G H (2013b). Landslides triggered by slipping-fault-generated earthquake on a plateau: an example of the 14 April 2010, Ms 7.1, Yushu, China earthquake. Landslides, 10(4): 421–431

Xu C, Xu X W, Zheng W J (2013c). Compiling inventory of landslides triggered by Minxian-Zhangxian earthquake of July 22, 2013 and their spatial distribution analysis. Journal of Engineering Geology, 21 (5): 736–749 (in Chinese)

Xu C, Xu X W, Zheng W J, Min W, Ren Z K, Li Z Q (2013d). Landslides triggered by the 2013 Minxian-Zhangxian, Gansu Province Ms 6.6 Eartqhuake and its tectonic analysis. Seismology and Geology, 35(3): 616–626 (in Chinese)

Xu X W, Wen X Z, Yu G H, Chen G H, Klinger Y, Hubbard J, Shaw J (2009a). Coseismic reverse-and oblique-slip surface faulting generated by the 2008 Mw 7.9 Wenchuan earthquake, China. Geology, 37 (6): 515–518

Xu X W, Yu G H, Chen G H, Ran Y K, Li C X, Chen Y G, Chang C P (2009b). Parameters of coseismic reverse- and oblique-slip surface ruptures of the 2008 Wenchuan earthquake, eastern Tibetan Plateau. Acta Geologica Sinica-English Edition, 83(4): 673–684

Yalcin A (2008). GIS-based landslide susceptibility mapping using analytical hierarchy process and bivariate statistics in Ardesen (Turkey): comparisons of results and confirmations. Catena, 72(1): 1–12